Meckel's and condylar cartilages anomalies in achondroplasia result in defective development and growth of the mandible

Martin Biosse Duplan, Davide Komla-Ebri, Yann Heuzé, Valentin Estibals, Emilie Gaudas, Nabil Kaci, Catherine Benoist-Lasselin, Michel Zerah, Ina Kramer, Michaela Kneissel, et al.

▶ **To cite this version:**

Martin Biosse Duplan, Davide Komla-Ebri, Yann Heuzé, Valentin Estibals, Emilie Gaudas, et al.. Meckel's and condylar cartilages anomalies in achondroplasia result in defective development and growth of the mandible. Human Molecular Genetics, 2016, 25 (14), pp.2997-3010. ⟨10.1093/hmg/ddw153⟩. ⟨hal-02322596⟩

HAL Id: hal-02322596

https://hal.science/hal-02322596v1

Submitted on 11 Jan 2021

HAL is a multi-disciplinary open access archive for the deposit and dissemination of scientific research documents, whether they are published or not. The documents may come from teaching and research institutions in France or abroad, or from public or private research centers.

L'archive ouverte pluridisciplinaire **HAL**, est destinée au dépôt et à la diffusion de documents scientifiques de niveau recherche, publiés ou non, émanant des établissements d'enseignement et de recherche français ou étrangers, des laboratoires publics ou privés.

HAL Authorization

OXFORD

Human Molecular Genetics, 2016, Vol. 25, No. 14 2997–3010

doi: 10.1093/hmg/ddw153
Advance Access Publication Date: 3 June 2016
Original Article

ORIGINAL ARTICLE

Meckel's and condylar cartilages anomalies in achondroplasia result in defective development and growth of the mandible

Martin Biosse Duplan[1,2], Davide Komla-Ebri[1], Yann Heuzé[3], Valentin Estibals[1], Emilie Gaudas[1], Nabil Kaci[1], Catherine Benoist-Lasselin[1], Michel Zerah[4], Ina Kramer[5], Michaela Kneissel[5], Diana Grauss Porta[5], Federico Di Rocco[1,4,†] and Laurence Legeai-Mallet[1,6,*]

[1]INSERM U1163, Université Paris Descartes, Sorbonne Paris Cité, Institut Imagine, Paris, France, [2]Service d'Odontologie, Hôpital Bretonneau, HUPNVS, AP-HP, Paris, France, [3]UMR5199 PACEA, Université de Bordeaux, Bordeaux Archaeological Sciences Cluster Of Excellence, Université de Bordeaux, Bordeaux, France, [4]Neurochirurgie Pédiatrique, Unité de Chirurgie Craniofaciale, Hôpital Necker-Enfants Malades, AP-HP, Paris, France, [5]Novartis Institutes for BioMedical Research, Basel, Switzerland and [6]Service de Génétique, Hôpital Necker-Enfants Malades, AP-HP, Paris, France

*To whom correspondence should be addressed at: Phone: + 33 1 42754302; Fax: + 33 1 42754221; Email: laurence.legeai-mallet@inserm.fr

Abstract

Activating FGFR3 mutations in human result in achondroplasia (ACH), the most frequent form of dwarfism, where cartilages are severely disturbed causing long bones, cranial base and vertebrae defects. Because mandibular development and growth rely on cartilages that guide or directly participate to the ossification process, we investigated the impact of FGFR3 mutations on mandibular shape, size and position. By using CT scan imaging of ACH children and by analyzing *Fgfr3*$^{Y367C/+}$ mice, a model of ACH, we show that *FGFR3* gain-of-function mutations lead to structural anomalies of primary (Meckel's) and secondary (condylar) cartilages of the mandible, resulting in mandibular hypoplasia and dysmorphogenesis. These defects are likely related to a defective chondrocyte proliferation and differentiation and pan-FGFR tyrosine kinase inhibitor NVP-BGJ398 corrects Meckel's and condylar cartilages defects *ex vivo*. Moreover, we show that low dose of NVP-BGJ398 improves *in vivo* condyle growth and corrects dysmorphologies in *Fgfr3*$^{Y367C/+}$ mice, suggesting that postnatal treatment with NVP-BGJ398 mice might offer a new therapeutic strategy to improve mandible anomalies in ACH and others FGFR3-related disorders.

†Present address: Neurochirurgie Pédiatrique, Hopital Femme Mère Enfant CHU de Lyon, Université Claude Bernard Lyon 1, Lyon, France.
Received: April 13, 2016. **Revised:** May 12, 2016. **Accepted:** May 13, 2016

© The Author 2016. Published by Oxford University Press.
This is an Open Access article distributed under the terms of the Creative Commons Attribution Non-Commercial License (http://creativecommons.org/licenses/by-nc/4.0/), which permits non-commercial re-use, distribution, and reproduction in any medium, provided the original work is properly cited. For commercial re-use, please contact journals.permissions@oup.com

Introduction

Achondroplasia (ACH) is the most common form of chondrodysplasia and is characterized by a rhizomelic dwarfism with short limbs, macrocephaly, frontal bossing and midface hypoplasia (1–3). ACH is caused by an activating mutation of *Fibroblast Growth Factor Receptor 3* (*FGFR3*) that affects both endochondral and membranous ossification (3–5). FGFR3 overactivation disturbs the proliferation and differentiation of chondrocytes in the growth plate of long bones (6–8) and synchondroses of the cranial base (3,9). Other cartilaginous structures are affected in ACH, such as the inner ear (10), vertebral bodies and intervertebral disc (11) and joints (7).

Mandibular growth relies greatly on primary and secondary cartilages, even though their exact roles in the acquisition of the mandible final shape and size are not fully understood (12,13). Meckel's cartilage (MC) is a rod-shaped primary cartilage that runs through the mandibular process of the first pharyngeal arch and acts as a morphogenic template for the membranous ossification of the mandible body. It is transiently present in the developing mandible and disappears at birth. Secondary cartilages (symphyseal, angular and condylar cartilages) form prenatally and eventually ossify by endochondral ossification during post-natal growth, serving as growth centers (12). The central role of cartilages in mandibular development and growth is exemplified by the mandibular phenotype observed in several chondrodysplasias where mutations in genes involved in chondrocyte function, such as *Collagen II* (responsible for Achondrogenesis type II), *Sox9* (Campomelic dysplasia) or *PTHrP* (Jansen type of metaphyseal chondrodysplasia) result in abnormal mandibular shape, size or position (14–16).

Mutations of *FGFR1*, *FGFR2* and *FGFR3* genes are associated with various aspects of abnormal craniofacial development such as craniosynostoses and maxillary hypoplasia (2,17,18). FGFR2 and FGFR3 are expressed in MC (19,20) and throughout all phases of the chick mandibular development (21). FGFR3 signaling is required for the elongation of chick MC and FGFR2 and FGFR3 play a role during membranous ossification of mandible (22). Mandibular defects have also been observed in $Fgfr1/2^{dcko}$ mice, with a shorter and smaller mandible at birth (20). The deletion in mice of the FGFR3 signaling molecule Snail (23) is associated with a growth retardation of MC and a reduction in mandibular length (24) and mice deficient for the FGFR3 ligand FGF18 display a reduced size of MC and a hypoplastic mandible (25). These data support the role of FGFR signaling in the elongation of MC and morphogenesis of the mandible.

However, it is unknown whether mandibular growth and development are affected in children with ACH and whether mandibular cartilages are disturbed by FGFR3 mutations. Analysis of lateral cephalogram from adult ACH patients has shown a prognathic mandible (i.e. anteriorly displaced) (26,27). It has also been reported that in humans, other skeletal dysplasia caused by activating mutations of *FGFR3* can result in mandibular dysmorphogenesis as seen in thanatophoric dysplasia (TD) (28), and Muenke syndrome (MS) (29).

In this article, we studied the mandible growth and development in children with ACH and observed an abnormal shape, size and position of the mandible. We compared the human data with those obtained with a mouse model of ACH ($Fgfr3^{Y367C/+}$) (10), for which we analyzed MC and secondary cartilages of the mandible. We observed proliferation and differentiation defects in chondrocytes of the mandibular cartilages and a delay in the replacement of MC by bone. By targeting the excessive activity of FGFR3 with a tyrosine kinase inhibitor NVP-BGJ398 (30), in organ cultures, we corrected the modifications of size and shape of the mandibles. Using NVP-BGJ398 in vivo, we observed a strong improvement of the mandibular phenotype. Taken together, these data bring out anomalies of the mandible in ACH and its mouse model and offer new perspective of treatment for ACH.

Results

Achondroplasia results in mandibular hypoplasia and dysmorphogenesis

Although the craniofacial phenotype of patients with ACH has been described (2,3,26), no specific analysis of the mandible has been conducted. We took advantage of CT images acquired for assessment of risks for cervicomedullary-junction compression in infants with ACH ($n = 8$, mean age: 21.3 months) and compared these images with those of age-matched controls obtained after traumatic events ($n = 9$, mean age: 24.9 months). The length of the mandible, measured as the distance between condylion (Co) and gnathion (Gn), was significantly and consistently decreased in ACH patients compared to controls (−14%; $P < 0.05$; Fig. 1A and B). Mandibular body length [Gonion (Go) – Menton (Me)] and mandibular ramus length (Go – Co) were also significantly decreased in ACH children (−16%; $P < 0.01$ and −17%; $P < 0.05$, respectively).

The analysis of tridimensional coordinates of anatomical landmarks with geometric morphometrics (31) showed differences in mandible shape between ACH patients and controls. Principal components analysis (PCA) of the human mandible shape resulted in the separation of ACH patients and controls along PC1 accounting for 47% of total variance on the basis of shape features represented in Figure 1C. When compared with controls, mandibles of ACH children were characterized by a defective orientation and size of the ramus with prominent coronoid processes and relatively shorter condyles.

FGFR3 activation in mice results in mandibular hypoplasia and dysmorphogenesis

The role of Fgfr1 and Fgfr2 during mandibular development was demonstrated in mice with a mesenchyme-specific disruption of Fgfr1 and Fgfr2 (20), while the impact of an activating Fgfr3 mutation on the mandible has not been studied. Here, we compared the mandible size and shape of $Fgfr3^{Y367C/+}$ mice that accurately mimic ACH (3,10,32) with wild-type (WT) mice at different ages. We sacrificed pregnant mice to collect $Fgfr3^{Y367C/+}$ and control littermate embryos at gestational day E16.5 and E18.5. Mice were also sacrificed at postnatal day 0 and 21. The mandibles were dissected and stained with alcian blue for cartilage and alizarin red for mineralized tissue. We observed a significant reduction in the length of the mandible body in the mutant mice at all time-points: −11% $P < 0.005$, −9% $P < 0.005$, −10% $P < 0.005$, −16% $P < 0.0001$ compared with WT littermates at E16.5, E18.5, P0 and P21, respectively (Fig. 1D and E).

To identify potential dysmorphologies in $Fgfr3^{Y367C/+}$ mandibles in addition to the hypoplasia, we measured anatomical landmarks on three-dimensional (3D) reconstructed micro-CT images of P21 mandibles and analyzed their coordinates with geometric morphometrics. The PCA of the mandible shape resulted in the separation of $Fgfr3^{Y367C/+}$ mice and controls littermates along PC1 accounting for 78% of total variance on the basis of shape features (mainly located on the ramus) represented in Fig. 1F. Our results revealed that the shape changes

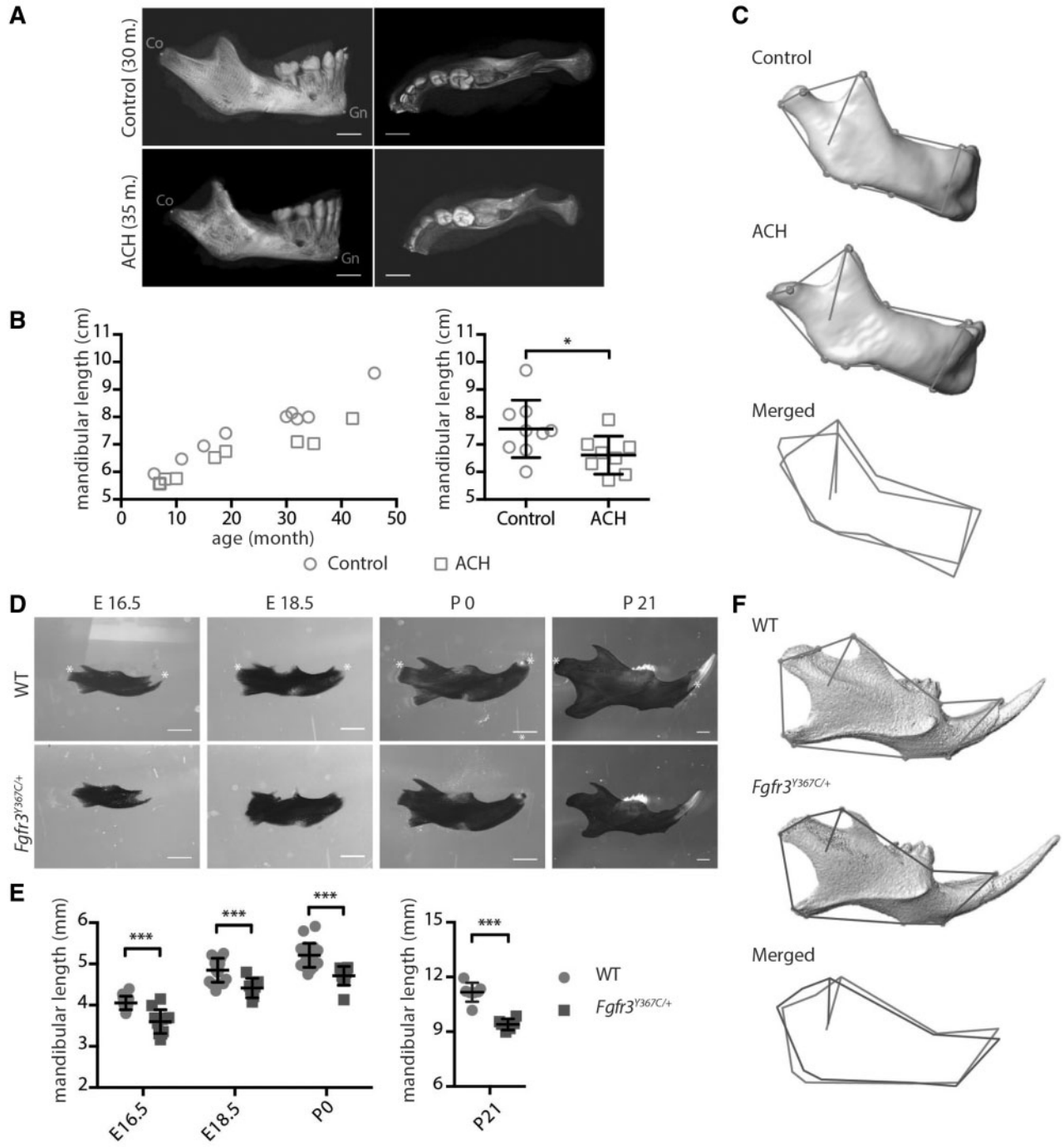

Figure 1. FGFR3 over activation in humans and mice results in mandibular hypoplasia and dysmorphogenesis. (**A**) 3D reconstructed CT images with volume rendering of a control and ACH patient (scale bar = 1 cm). (**B**) Mandible length, measured as the distance between condylion (Co) and gnathion (Gn) on sagittal sections of 3D reconstructed CT images of controls ($n = 9$, mean age: 24.9 months) or ACH patients ($n = 8$, mean age: 21.3 months) and plotted against the age of the children. (**C**) Landmarks and associated wireframes measured on the 3D reconstructed human mandibles and corresponding superimposition of the control and ACH wireframes computed on the basis of PC scores along PC1, the PC best separating the two groups and accounting for 47% of total shape variance. (**D** and **E**) Mandible length of embryos (E16.5 and E18.5), new born and 3-week-old WT and *Fgfr3*$^{Y367C/+}$ mice ($n \geq 6$ individuals for each age and genotype), measured following alcian blue and alizarin red staining between the condylar and symphyseal ends (marked with *) (scale bar = 1 mm). (**F**) Landmarks and associated wireframes measured on the 3D reconstructed mouse mandibles and corresponding superimposition of the control and *Fgfr3*$^{Y367C/+}$ wireframes computed on the basis of PC scores along PC1, the PC best separating the two groups and accounting for 78% of total shape variance. Data shown as mean with SD; *$P < 0.05$, ***$P < 0.005$.

observed in ACH patients, and *Fgfr3*$^{Y367C/+}$ mice were relatively similar.

Chondrocytes homeostasis is disturbed in MC of *Fgfr3*$^{Y367C/+}$ mice

We hypothesized that Fgfr3 activation disturbs chondrocytes homeostasis in MC, as it was shown in other cartilages, such as the growth plate (10), the inner ear (10), the cranial base synchondroses (3) or vertebral bodies (11), and that these defects could be responsible for the mandibular hypoplasia and dysmorphogenesis observed in *Fgfr3*$^{Y367C/+}$ mice. We therefore collected embryos at gestational day E16.5 and E18.5 and analyzed markers of chondrocyte proliferation and differentiation on histological sections.

At E16.5, MC was readily identifiable on sections stained with safranin'O (Fig. 2A). We focused on the cartilage within the developing mandible. In its central part, chondrocytes are organized into layers (33,34), as in a growth plate or a synchondrosis. We used several markers to compare the spatial organization of the chondrocytes into distinct zones in WT and mutant embryos and observed that the chondrocyte differentiation was disrupted in mutant embryos. First, immunostaining for Collagen X showed that the size of the hypertrophic chondrocytes zone relative to the total size of the cartilage was reduced (−43% compared to WT, $P < 0.05$; Fig. 2A and B), as was the size of individual hypertrophic chondrocytes (−51% compared to WT, $P < 0.0001$; Fig. 2A and C) in *Fgfr3*$^{Y367C/+}$ embryos. Immunostaining of the proliferation marker Ki67 indicated that more cells were proliferating in MC of mutant embryos (+81% compared to WT, $P < 0.01$; Fig. 2A and D). In WT and *Fgfr3*$^{Y367C/+}$ embryos, the zones of proliferating and hypertrophic cells were clearly delimited and were almost completely mutually exclusive (Fig. 2A). We then observed that the number of Fgfr3-positive cells in this cartilage was increased in *Fgfr3*$^{Y367C/+}$ embryos (+151%, $P < 0.0001$; Fig. 2A and D) as reported in the growth plate of the same mouse model (11,35) and ACH and TD fetuses (6). FGFR3 exhibits a specific pattern of expression during chondrocyte differentiation (5,36), and in the growth plate, its expression is mostly limited to the resting, proliferating and pre-hypertrophic chondrocytes (37). In WT embryos, Fgfr3 was expressed by proliferative and prehypertrophic chondrocytes (Fig. 2A), whereas in *Fgfr3*$^{Y367C/+}$ embryos, the pattern of expression was less clearly delimited, with an overlapping of Collagen X and Fgfr3-positive cartilage areas.

Differentiation into hypertrophic chondrocytes precedes and contributes to the disappearance of MC and replacement by bone (38,39). At E18.5, large remnants of cartilage were detected in *Fgfr3*$^{Y367C/+}$ embryos, in contrast with WT embryos where MC was mostly replaced by bone (Fig. 2E and F) and the size of MC was significantly increased in *Fgfr3*$^{Y367C/+}$ embryos mandible (+129%, $P < 0.05$). Similar defects lead to an ossification delay in the growth plate (40).

Overall, these results suggest that Fgfr3 constitutive activation disturbed the chondrocytes proliferation and differentiation and delayed the ossification process in MC.

FGFR3 activation reduces condylar growth in humans and mice

Deviations in the growth of the mandibular condyle can have major functional and aesthetic consequences (41). Although the majority of the mandible is formed by membranous ossification, the upper part of the ramus is formed by endochondral ossification of the condylar cartilage. This process allows the mandible to elongate and grow upward and backward (42). In both humans and mice, endochondral ossification is severely disturbed by *FGFR3* activating mutations and defects in condylar cartilage could contribute to mandibular hypoplasia and dysmorphogenesis. For these reasons, we characterized the condylar process, first in children with ACH, then in *Fgfr3*$^{Y367C/+}$ mice. We observed on sagittal sections from CT images that the length of the condylar neck in children with ACH was reduced compared to age-matched controls (−21%, $P < 0.005$; ACH: $n = 12$, mean age = 32.4 months; controls: $n = 14$, mean age = 32.4 months) (Fig. 3A and B). This reduction was observed in children aged from 1 to 42 months. In *Fgfr3*$^{Y367C/+}$ mice (P21), condylar hypoplasia was also present (Fig. 3C and D). In mutant mice, condyles were significantly reduced in length (−14.2%, $P < 0.01$) and width (−15.8%, $P < 0.001$).

To identify the mechanism that led to this shorter condylar neck, we examined the condylar cartilage on histological sections of E16.5 embryos and P21 mice. In *Fgfr3*$^{Y367C/+}$ mice, the size of the hypertrophic zone in the cartilage was reduced compared to WT littermates as was the average size of individual hypertrophic chondrocytes (E16.5: −48%, $P < 0.001$; P21: −56,3%, $P < 0.05$) (Fig. 3E–H).

Tyrosine kinase inhibition corrects primary and secondary cartilages defects in *Fgfr3*$^{Y367C/+}$ embryos

To test the hypothesis that the mandibular hypoplasia and dysmorphogenesis observed in children with ACH and *Fgfr3*$^{Y367C/+}$ mice are direct consequences of an overactive FGFR3, we analyzed the effect on mandibular development and growth of pharmacological inhibition of FGFRs using NVP-BGJ398, a pan-specific FGFR inhibitor (30). We first developed an *ex vivo* system of mandible explant cultures, similar to the femur explant cultures we used to test pharmacological approaches of FGFR inhibition (11,32,35). We isolated the mandible from WT and *Fgfr3*$^{Y367C/+}$ embryos at E16.5, dissected the mandibles into two hemi-mandibles and cultured those separately for 6 days. One hemi-mandible was treated with NVP-BGJ398, whereas the other served as control. As expected, the body and condyle of hemi-mandible from *Fgfr3*$^{Y367C/+}$ embryos treated with DMSO were smaller than those of WT hemi-mandibles also treated with DMSO (−10,1%, $P < 0.05$; −18%, $P < 0.05$ respectively, Fig. 4A and B). Incubation with NVP-BGJ398 of *Fgfr3*$^{Y367C/+}$ hemi-mandibles led to an increase in mandible body (+11%, $P < 0.05$) and condylar neck (+26%, $P < 0.05$) size, reaching the size of cultured WT hemi-mandibles treated with DMSO (Fig. 4A and B).

Increases in mandible length with NVP-BGJ398 treatment were associated with the correction of chondrocyte defects observed in primary and secondary mandibular cartilages of *Fgfr3*$^{Y367C/+}$ embryos. Although the size of MC hypertrophic zone relative to the size of the cartilage was clearly reduced in *Fgfr3*$^{Y367C/+}$ hemi-mandible treated with DMSO compared to WT (−40.2%, $P < 0.05$), this zone expanded following Fgfr3 inhibition in mutant mandible (+68.3%, $P < 0.05$) (Fig. 4C and D). This expansion was associated with an increased size of individual hypertrophic chondrocytes in hemi-mandible from *Fgfr3*$^{Y367C/+}$ embryos treated with NVP-BGJ398 (+165% compared to *Fgfr3*$^{Y367C/+}$ treated with DMSO, $P < 0.0001$) (Fig. 4C and E). We noted an increased replacement of MC by bone in the treated mandibles, compared to the untreated *Fgfr3*$^{Y367C/+}$ mandible, rescuing the extinction delay of MC observed

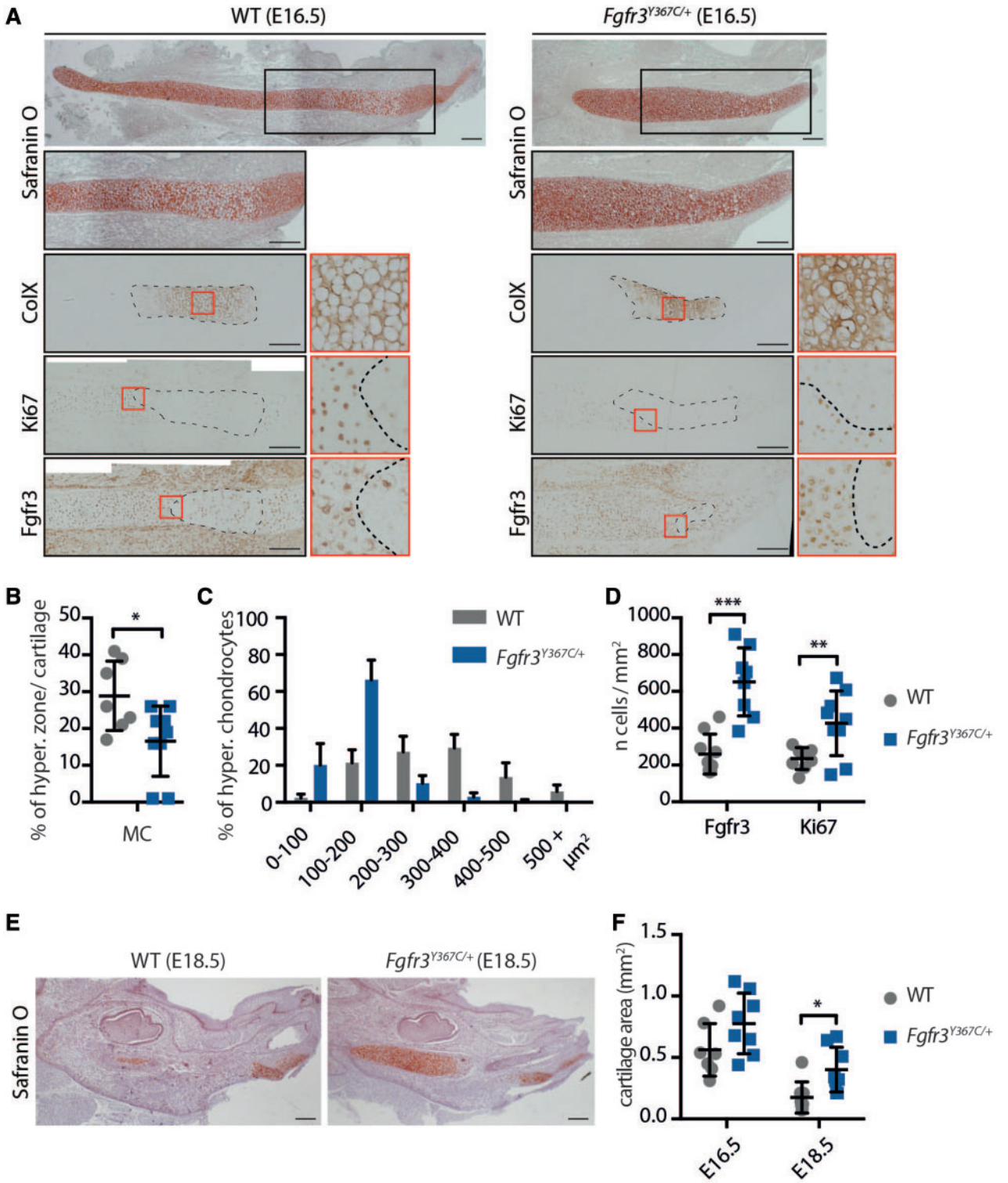

Figure 2. Chondrocytes homeostasis is disturbed in Meckel's cartilage of *Fgfr3*$^{Y367C/+}$ mice. (**A**) Histological staining (Safranin'O) and immunostaining for Collagen X, Ki67 (proliferation marker) and Fgfr3 of MC of WT and *Fgfr3*$^{Y367C/+}$ E16.5 embryos. An enlargement of the ColX immunostaining (red box) highlights the modification in the size of hypertrophic chondrocytes in *Fgfr3*$^{Y367C/+}$ embryos (scale bar = 200 µm). Area delimited with doted lines on the ColX panel corresponds to the hyperthrophic zone. Areas delimited with doted lines on the Ki67 and Fgfr3 panels correspond to immunonegative zones (respectively non-proliferative and Fgfr3-negative). Enlargements of the Ki67 and Fgfr3 immunostainings (red box) highlight the limits of the positive and negative zones. (**B**) Measurement of the ColX positive zone inside MC of WT and *Fgfr3*$^{Y367C/+}$ E16.5 embryos ($n \geq 7$ individuals for each genotype). (**C**) Mean percentage of hypertrophic chondrocytes for different size categories (expressed in µm²) inside MC of WT and *Fgfr3*$^{Y367C/+}$ E16.5 embryos ($n \geq 50$ cells from $n \geq 6$ individuals for each genotype). (**D**) Mean number of immuno-positive cells for Fgfr3 or Ki67 inside MC of WT and *Fgfr3*$^{Y367C/+}$ E16.5 embryos ($n \geq 7$ individuals for each genotype). (**E**) Histological staining (Safranin'O) of WT and *Fgfr3*$^{Y367C/+}$ E18.5 embryos (scale bar = 200 µm). (**F**) Mean cartilage area, measured on sagittal sections of MC in WT and *Fgfr3*$^{Y367C/+}$ E16.5 and E18.5 embryos ($n \geq 7$ individuals for each age and genotype). Data shown as mean with SD; $^{*}P < 0.05$, $^{**}P < 0.01$, $^{***}P < 0.005$.

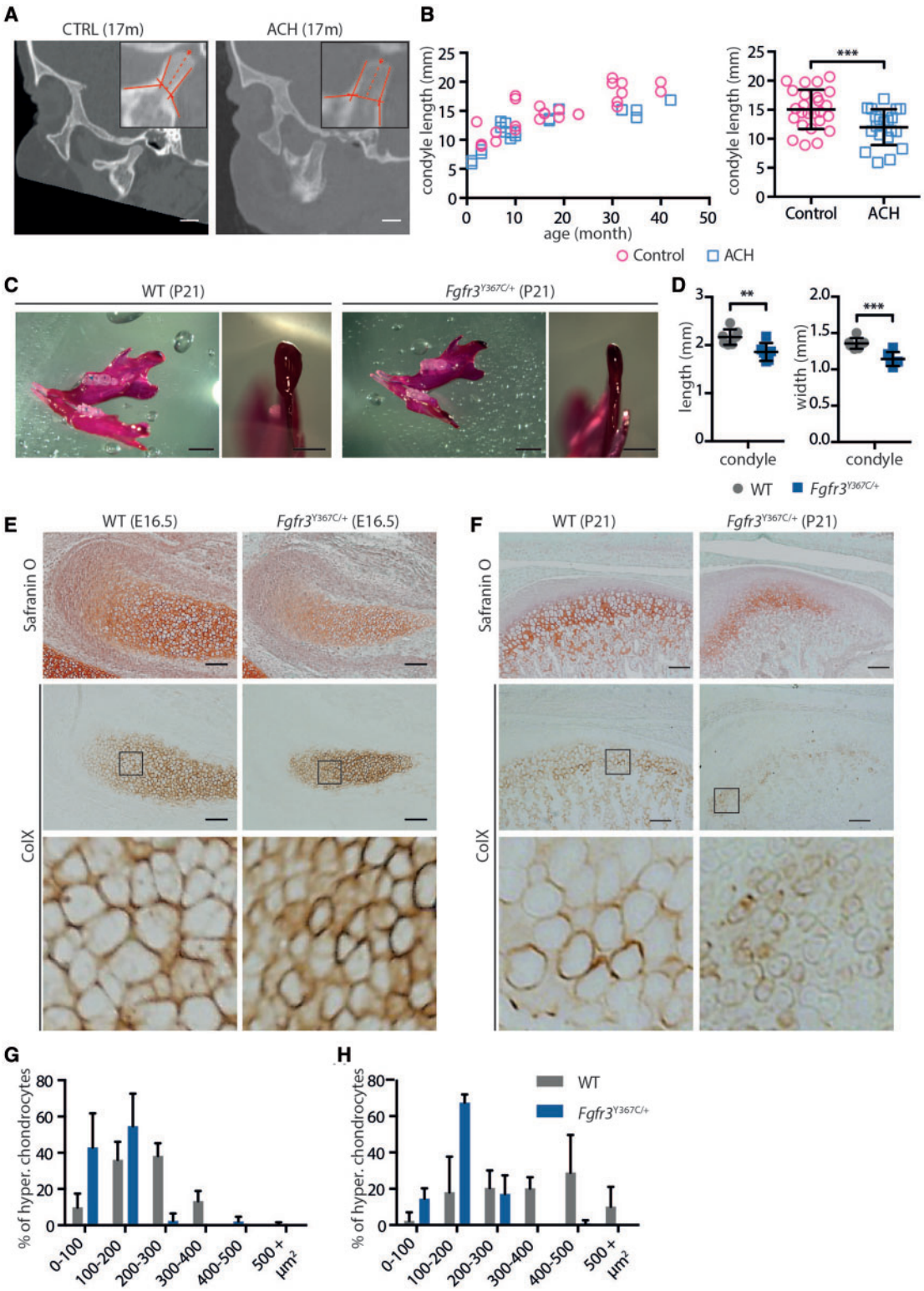

Figure 3. FGFR3 over-activation in humans and mice results in condyle hypoplasia. (**A**) Representative sagittal sections of a control and ACH child, both 17 months of age, generated from the CT scans (scale bar = 1 cm). (**B**) Condylar neck length, measured on CT scans sagittal sections of controls ($n = 14$, mean age = 32.4 months) or ACH patients ($n = 12$, mean age = 32.4 months) and plotted against the age of the children. (**C**) Representative macroscopic views of condyles of 3-week-old WT and *Fgfr3*$^{Y367C/+}$ mice, following alcian blue and alizarin red staining (scale bars = 2 and 1 mm). (**D**) Condylar neck length of 3-week-old WT and *Fgfr3*$^{Y367C/+}$ mice, measured following alcian blue and alizarin red staining ($n \geq 6$ individuals for each genotype). (**E** and **F**) Histological staining (Safranin'O) and immunostaining for Collagen X of the condylar cartilage of WT and *Fgfr3*$^{Y367C/+}$ E16.5 embryos (E) and 3-week-old mice (F) (scale bar = 100 µm). An enlargement of the ColX immunostaining (black box) highlights the modification in the size of hypertrophic chondrocytes in *Fgfr3*$^{Y367C/+}$ embryos and P21 mice. (**G** and **H**) Mean percentage of hypertrophic chondrocytes for different size categories (expressed in µm^2) inside the condylar cartilage of WT and *Fgfr3*$^{Y367C/+}$ E16.5 embryos (G) and 3 weeks old mice (H) ($n \geq 50$ cells from $n \geq 6$ individuals for each age and genotype). Data shown as mean with SD; $^{**}P < 0.01$, $^{***}P < 0.005$.

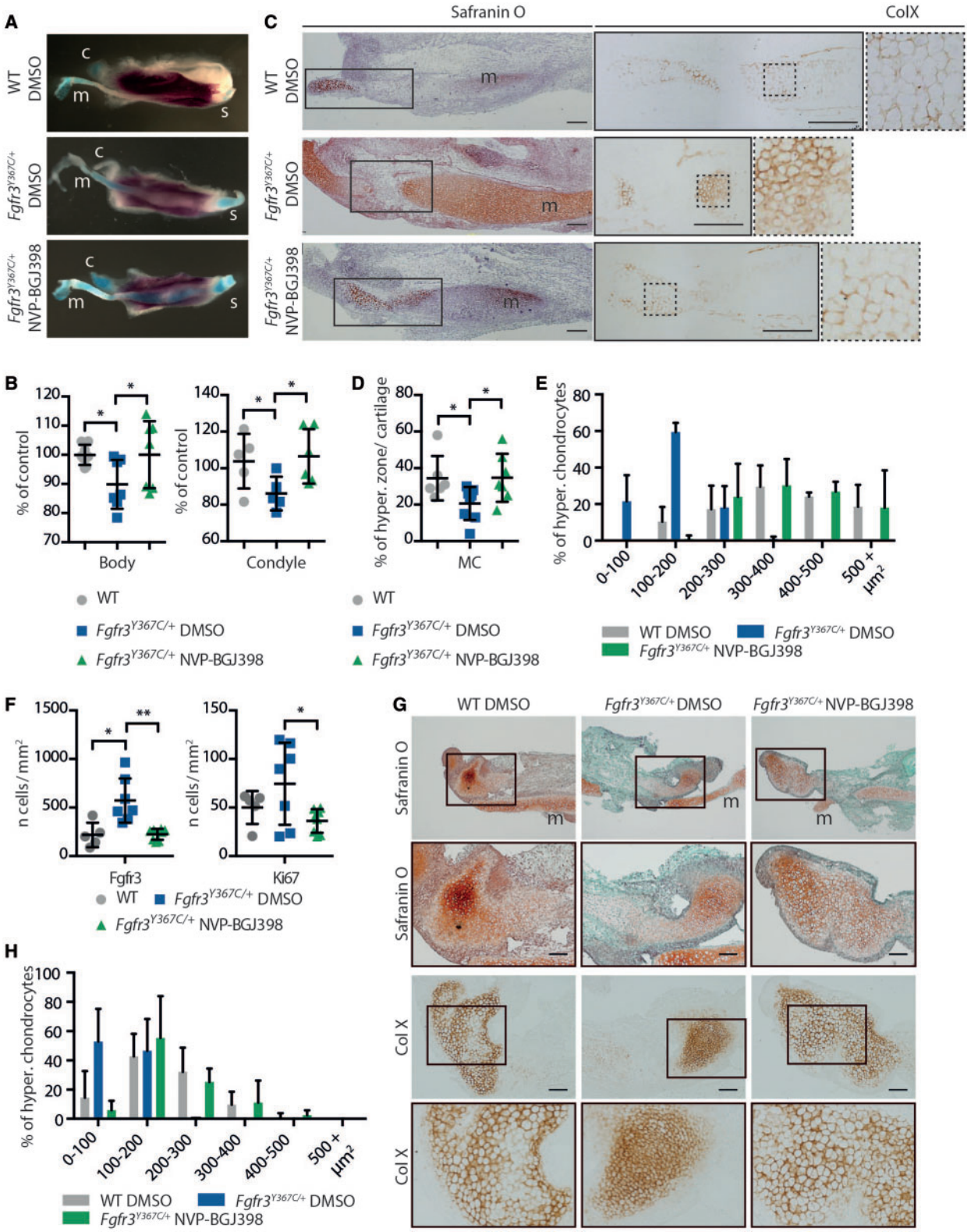

Figure 4. NVP-BGJ398 corrects primary and secondary cartilages defects in *ex vivo* cultures of mandibles from *Fgfr3*$^{Y367C/+}$ embryos. (**A**) Representative macroscopic views of hemi-mandibles from E16.5 WT or *Fgfr3*$^{Y367C/+}$ embryos, treated with DMSO or NVP-BGJ398 and cultured for 6 days, following alcian blue and alizarin red staining. Symphyseal (s), condylar (c) and Meckel's (m) cartilages are indicated. (**B**) Mandibular body and condylar neck length of cultured hemi-mandibles ($n \geq 5$ individuals for each genotype and treatment). Total length of the hemi-mandible was measured as well as the length of the condylar and symphyseal cartilages (identified with the alcian blue staining). The length of the body was calculated as the total length minus the condylar and symphyseal cartilages. (**C**) Histological staining (Safranin'O) and immunostaining for ColX of cultured hemi-mandibles. An enlargement of the ColX immunostaining highlights the modification in the size of hypertrophic chondrocytes in MC of *Fgfr3*$^{Y367C/+}$ embryos and the correction of the defect with NVP-BGJ398 (scale bar = 200 µm). (**D**) Measurement of the ColX positive zone inside MC of

in *Fgfr3*$^{Y367C/+}$ mice. The kinase inhibitor also corrected the overexpression of Fgfr3 and the increased proliferation of chondrocytes in MC of *Fgfr3*$^{Y367C/+}$ hemi-mandible (Fig. 4F).

In the condylar cartilage, similar changes were observed. Treatment with NVP-BGJ398 increased the size of the cartilage hypertrophic zone and the size of individual hypertrophic chondrocytes in condyles of *Fgfr3*$^{Y367C/+}$ embryos (+98.4%, $P < 0.0005$ compared to condyles from *Fgfr3*$^{Y367C/+}$ hemi-mandibles treated with DMSO) (Fig 4G and H).

Altogether, we observed that the reduction of Fgfr3 activity with NVP-BGJ398 corrected the defective growth and cellular defects observed in the presence of an overactive Fgfr3. As those improvements occurred in the absence of any systemic regulation (*ex vivo* explants), the effect of the inhibitor is likely direct. This reinforces the view that the cartilage defects are responsible for the mandibular hypoplasia.

Tyrosine kinase inhibition improves the mandibular dysmorphogenesis and the size of the condyle in *Fgfr3*$^{Y367C/+}$ mice

Finally, we tested the potential benefit of a pharmacological use of tyrosine kinase inhibitor to correct *in vivo* the mandibular hypoplasia and dysmorphogenesis of *Fgfr3*$^{Y367C/+}$ mice. We performed daily subcutaneous injection of either NVP-BGJ398 (2 mg/kg) or vehicle on 1-day-old mice from P0 to P15 (11). The mandibles of P16 mice were then imaged by micro-CT. As in the *ex vivo* experiments, we observed phenotypic changes of the condylar neck in *Fgfr3*$^{Y367C/+}$ mice treated with NVP-BGJ398 compared to *Fgfr3*$^{Y367C/+}$ littermates treated with DMSO. The length (+20.9%, $P < 0.005$) and width (+22%, $P < 0.005$) of the condylar neck were increased by the reduction of the overactivation of FGFR3 ($n = 7$, $n = 8$ and $n = 7$ for WT vehicle, *Fgfr3*$^{Y367C/+}$ vehicle and *Fgfr3*$^{Y367C/+}$ NVP-BGJ398, respectively) (Fig. 5A and B). As expected, the length of mandible body was unchanged because MC had already been replaced by bone at the start of the injections. We confirmed the positive effect of NVP-BGJ398 on condylar cartilage with histological sections of the condyles (Fig. 6A and B). The PCA of the Procrustes shape coordinates of the landmarks measured on all mandibles was also run. As for P21 mice, PC1 separated the WT vehicle and the *Fgfr3*$^{Y367C/+}$ vehicle mice (Fig. 5C and D). The *Fgfr3*$^{Y367C/+}$ NVP-BGJ398 mice occupied a somewhat intermediate position though they overlap with the *Fgfr3*$^{Y367C/+}$ vehicle mice (Fig. 5C and D). *P*-values from permutation tests (10 000 permutation rounds) for Mahalanobis distances among groups showed that the *Fgfr3*$^{Y367C/+}$ NVP-BGJ398 mice were significantly different in

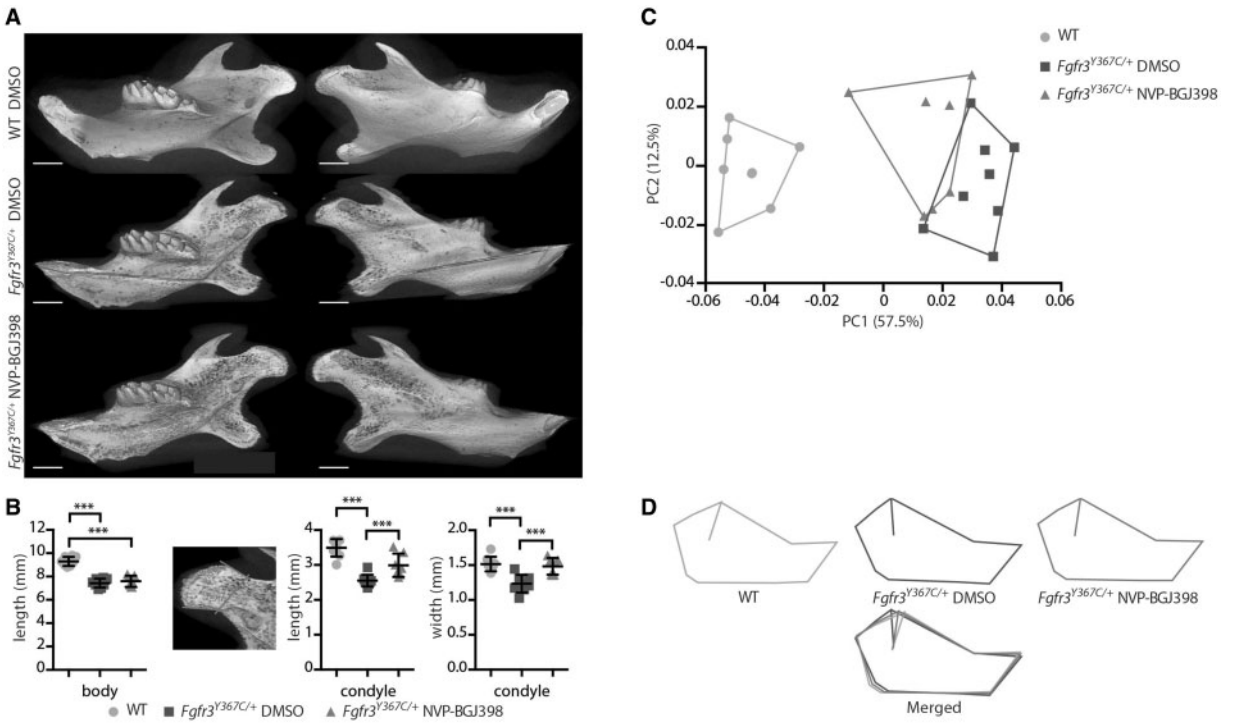

Figure 5. NVP-BGJ398 improves *in vivo* condyle growth of *Fgfr3*$^{Y367C/+}$ mice. (**A**) Representative 3D reconstructions of 16-day-old WT and *Fgfr3*$^{Y367C/+}$ mice treated with DMSO or NVP-BGJ398 for 15 days since P01 (scale bar = 1 mm). (**B**) Measurement of the mandible body and the condyle length and width of WT and *Fgfr3*$^{Y367C/+}$ mice treated with DMSO or NVP-BGJ398 ($n \geq 6$ individuals for each genotype and treatment). Total length of the mandible and the length of the condyle were measured . The length of the body was calculated as the total length minus the condyle. (**C** and **D**) PCA of the Procrustes shape coordinates of the landmarks measured on mandibles of WT and *Fgfr3*$^{Y367C/+}$ mice treated with DMSO or NVP-BGJ398 and corresponding superimposition ($n \geq 6$ individuals for each genotype and treatment). Data shown as mean with SD; ***$P < 0.005$.

cultured hemi-mandibles ($n \geq 6$ individuals for each genotype and treatment). (**E**) Mean percentage of hypertrophic chondrocytes for different size categories (expressed in μm^2) inside MC of cultured hemi-mandibles ($n \geq 50$ cells from $n \geq 5$ individuals for each genotype and treatment). (**F**) Mean number of immune positive cells for Fgfr3 or Ki67 inside MC of WT, *Fgfr3*$^{Y367C/+}$ DMSO and *Fgfr3*$^{Y367C/+}$ NVP-BGJ398 E16.5 embryos ($n \geq 5$ individuals for each genotype). (**G**) Histological staining (Safranin'O) and immunostaining for Collagen X of cultured hemi-mandibles condylar cartilage (scale bar = 100 μm). Meckel's cartilage (m) is indicated. (**H**) Mean percentage of hypertrophic chondrocytes for different size categories (expressed in μm^2) inside condylar cartilage of cultured hemi-mandibles ($n \geq 50$ cells from $n \geq 5$ individuals for each genotype and treatment). Data shown as mean with SD; *$P < 0.05$, **$P < 0.01$.

the shape of the mandible from either the *Fgfr3*$^{Y367C/+}$ vehicle mice or the WT vehicle. When comparing the centroid size (CS) used as a proxy for overall size of the mandible, WT mice displayed significantly larger mandible than *Fgfr3*$^{Y367C/+}$ mice treated with the vehicle ($t = -6.96$; $P < 0.005$) or NVP-BGJ398 ($t = -7.35$; $P < 0.005$). *Fgfr3*$^{Y367C/+}$ NVP-BGJ398 mice did not display significantly larger mandible than the *Fgfr3*$^{Y367C/+}$ vehicle mice ($t = -0.0887$; $P = 0.931$). These data confirm that the length of the mandible was not corrected by the treatment, but that the overall shape of the mandible of *Fgfr3*$^{Y367C/+}$ was improved with NVP-BGJ398.

Discussion

Deviation from normal mandible growth can strongly affect the masticatory and respiratory functions, speech and aesthetic appearance of the face (41,43), and mandibular cartilages are

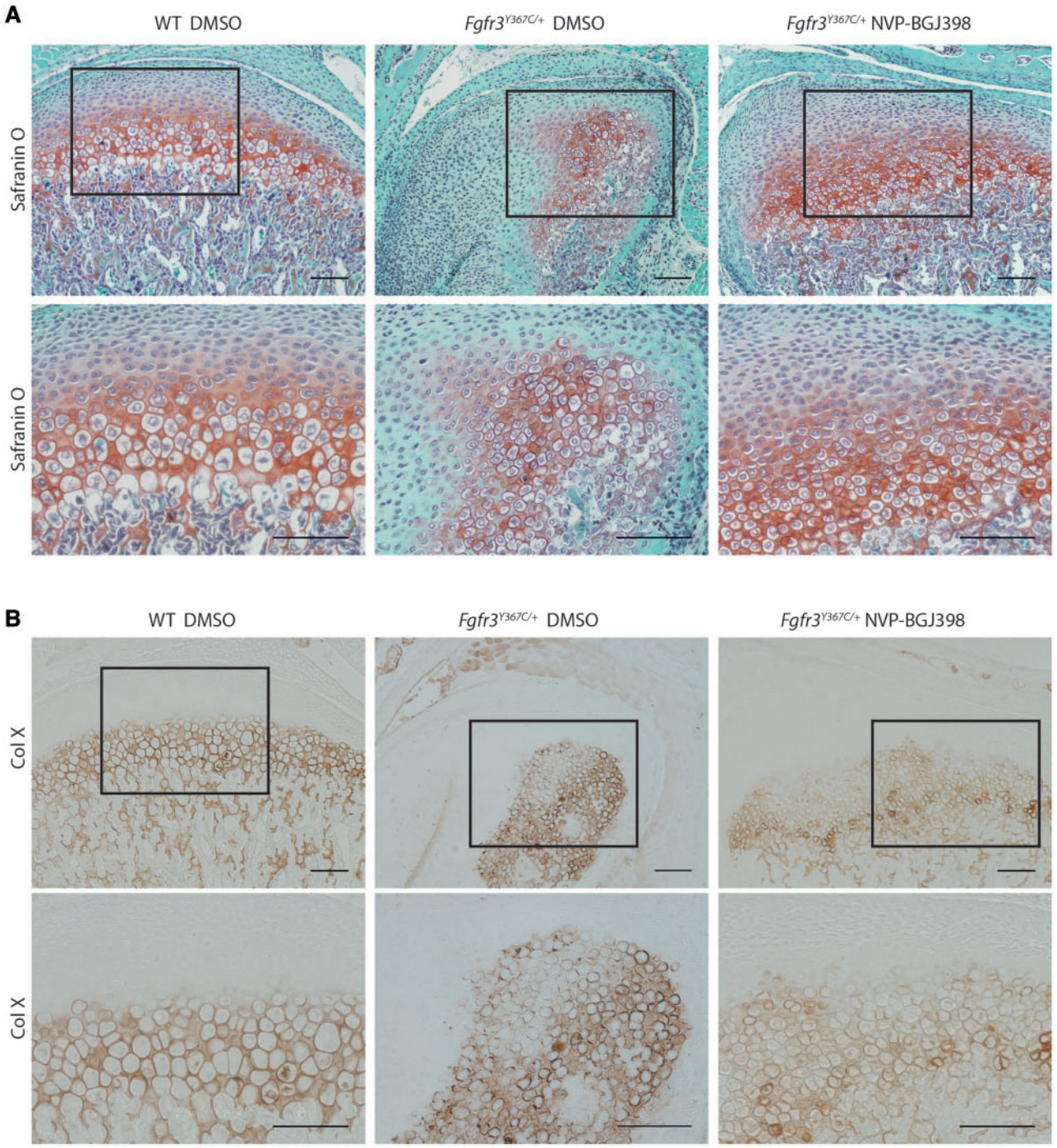

Figure 6. NVP-BGJ398 improves *in vivo* the chondrocyte differentiation in condyle of *Fgfr3*$^{Y367C/+}$ mice. Histological staining (Safranin'O) (**A**) and immunostaining for collagen X (**B**) of condylar cartilage of 16-day-old WT and *Fgfr3*$^{Y367C/+}$ mice treated with DMSO or NVP-BGJ398 for 15 days since P01 (scale bar = 100 μm).

recognized as critical growth centers for the mandible. Although many cartilages are affected in *FGFR3*-related chondrodysplasias, most strikingly the cartilaginous growth plate in the growing skeleton, mandibular cartilages and their impact on mandible growth had never been investigated in ACH. Our hypothesis was that mandibular cartilages would be affected by *FGFR3*-activating mutations, similar to other cartilages, and that these defects would cause modifications in the shape, size and/or position of the mandible.

We first observed differences in the size and shape of the mandible between ACH and control children. The mandible as a whole, or subunits such as the mandibular body and ramus were reduced in size at all ages in children with ACH and morphometric analysis revealed modifications in the shape of the ramus. Comparable changes were present in $Fgfr3^{Y367C/+}$ mice, and in both children and mice, the mandibular hypoplasia worsened with age. Our findings illustrate again the similarity of this mouse model with ACH.

In addition to ACH, *FGFR3*-activating mutations cause four other types of chondrodysplasia (hypochondroplasia, severe achondroplasia with developmental delay and acanthosis nigricans, and TD type I and II) (1,2) and two types of craniosynostoses (MS and Crouzon syndrome with acanthosis nigricans) (44). The presence of mandible abnormalities in these diseases has rarely been studied. A report showed mandibular clefting in a case of TD I (28), two cephalometric studies in adult ACH patients reported opposite results concerning the size of the mandible [normal for Cohen *et al.* (26) or decreased for Cardoso *et al.* (27)], whereas another study showed that MS patients had shorter mandibular body length than controls (29). Several mouse lines carrying *Fgfr3* activating mutations have been generated but a very few comprehensive analysis of the mandible are available. The homozygous *Fgfr3* G380R mouse, a model for ACH, has a reduced mandible length (79% of controls) (45), and the homozygous *Fgfr3* P244R mouse, a model for MS, has a hypomorphic condyle (46).

The *FGFR3* mutations responsible for chondrodysplasias and craniosynostoses were until recently known to primarily affect different ossification processes (endochondral versus membranous), but as observed in ACH (3), FGFR3 over-activation can consistently disturbs both ossification processes. The ossification of the mandible relies on these two types, the body being formed by membranous ossification, whereas the ramus is mainly formed by endochondral ossification. If the effect of *FGFR3* mutations responsible for ACH on the ramus is expected, it is intriguing that the same mutations can affect the size of the mandibular body. In order to understand what led to these changes we studied a primary (Meckel's) and a secondary (condylar) cartilage. The exact role of MC is not yet fully understood as it disappears before birth and only marginally participates in the ossification process of the mandible (47). It could play a role in the elongation of the mandible body as exemplified by the severe micrognathia present when MC is strongly perturbed as in the case of *Sox9* haploinsufficiency (48) or deletion of Snai1 and Snai2 (24). Here, we found that Fgfr3 over-activation disturbed the differentiation of chondrocytes in MC. The size of the hypertrophic zone was markedly shortened, as was the size of individual hypertrophic chondrocytes. The same defects were observed in the growth plate of ACH patients (6) and $Fgfr3^{Y367C/+}$ mice (10,40). As the chondrocytes differentiate in the growth plate, the volume enlargement to become hypertrophic determines the size of the growth plate elongation (49–51). The same mechanism could occur in MC and the disruption of MC chondrocytes differentiation caused by FGFR3 over-activation could lead to the shortening of the mandible body. Supporting this view, we observed that reduction of the tyrosine kinase activity of FGFR3 with NVP-BGJ398 not only corrected the hypertrophic chondrocyte phenotype in mandible *ex vivo* cultures but also improved the shortening of the mandible of $Fgfr3^{Y367C/+}$ embryos. In contrast, the same molecule had no effect on the mandible body once MC was replaced by bone. We assume that this is due to the disappearance of MC before birth and, to us, reinforces the importance of MC in the elongation of the mandible. In mice of this age, ossification of the symphyseal is limited and therefore contributes marginally to the elongation of the mandible body (52).

The activity of FGFR3 must be precisely tuned for normal mandible elongation because the injection of dominant negative (DN) form of FGFR3 in the chick embryo leads to the truncation or shortening of MC (22). In the same study, the DN form reduced the proliferation of the cells in MC, whereas in our study, we observed that it was markedly increased by the activating mutation. Increased chondrocyte proliferation was also observed in the growth plate of embryos carrying either the *Fgfr3* Y367C or K644E mutations (40,53). In MC, the expression of Fgfr3 was also increased by the Y367C *Fgfr3* mutation. It could be the result of a prolonged half time of the protein because the mutation of the transmembrane domain could delay the turnover and degradation of the activated receptor (54,55).

FGFR3 mutations responsible for ACH could also affect the ossification of the mandibular process that was delayed in $Fgfr3^{Y367C/+}$ embryos. It could be a consequence of the defective MC homeostasis and subsequent initiation of ossification. Alternatively, mesenchymal cells lateral to MC that directly differentiate into osteoblasts (20) could be independently affected by FGFR3 activation. Further work is needed to determine whether this delay affects mandible bone mass acquisition during growth, as reported in long bones (40,56).

Secondary cartilages are sites of late prenatal and early postnatal growth and eventually ossify. Here, we focused on the condylar cartilage. It develops adjacent to the intramembranous bone of the mandible, distinct from MC and in contrast with MC, directly contributes to the formation of the ramus by endochondral ossification and persists postnatally to function as a growth center (42). Genetic defects in chondrogenesis can cause abnormal condylar growth as in Pierre Robin sequence (41), an entity associated with genetic defects of SOX9 (57). We found that children with ACH had shorter condylar neck, a feature also found in $Fgfr3^{Y367C/+}$ mice. Histological analysis of the condyle in $Fgfr3^{Y367C/+}$ mice revealed a disturbed cartilage where the hypertrophic chondrocytes were smaller and the hypertrophic zone shortened, as in MC or in the growth plate of the same mice (10). Altered differentiation of chondrocyte is also present in condyles of TD infants (58) and in the hypolpastic condyle of homozygous *Fgfr3* P244R mice (46). Here, cultures of hemi-mandibles and in vivo experiments with partial inhibition of Fgfr3 activity showed that it is likely that the defective chondrocyte differentiation and proliferation directly contributes to the reduced elongation of the condyle. The persistence of the condylar cartilage postnatally allowed us to observe that *in vivo* tyrosine kinase inhibition rescue condylar growth in $Fgfr3^{Y367C/+}$ mice, increasing its length by 21% after 15 days of treatment. The same treatment improved the growth of appendicular and axial skeletons with a similar magnitude of change of long bones (11).

Current treatments of maxillofacial deformities and skeletal dysplasia are primarily surgical and can require multiple interventions during childhood (59,60). Innovative pharmacological

treatments of these diseases are needed and reducing the excessive activity of the FGFR3 receptor in *FGFR3*-related chondrodysplasias or craniosynostoses with specific tyrosine kinase inhibitors, such as NVP-BGJ398, is an appealing approach. It potentially targets all downstream signaling pathways of the receptor, and in this aspect, NVP-BGJ398 has been shown to normalize *in vitro* and *in vivo* ERK1/2 and PLCγ pathways (11). Our pre-clinical experiments showed here that this inhibitor enters mandibular cartilages and improves craniofacial growth.

In summary, we showed in this article that a *FGFR3* gain-of-function mutation disturbs the development and growth of the mandible, via structural anomalies of Meckel's and condylar cartilages. These anomalies are likely related to the defective chondrocyte proliferation and differentiation, and the tyrosine kinase inhibitor NVP-BGJ398 corrects these defects and improves condyle growth. This suggests that postnatal treatment with the molecule could be a therapeutic strategy to improve mandible growth in ACH and others FGFR3-related disorders.

Materials and Methods

Human subjects

All patients with ACH ($n = 12$, mean age = 32.4 months) or age-matched controls ($n = 14$, mean age = 32.4 months) were examined and followed at the Craniofacial Surgery Unit of Necker-Enfants Malades Hospital. Ethics approvals were obtained from the institutional review Board of Necker-Enfants Malades Hospital.

Mouse models

All the experiments were conducted in *Fgfr3*$^{Y367C/+}$ mice, a mouse model that display parts of the clinical hallmarks of ACH (32), or WT littermates, used as controls. WT and *Fgfr3*$^{Y367C/+}$ mice were generated by crossing *Fgfr3*^{neoY367C} mice (10) and *Cmv-Cre* mice (61). The mutant mice express the c.1100A > G (p.Tyr367Cys) mutation corresponding to the c.1118A > G (p.Tyr373Cys) in TD. All mice were on a C57BL/6 background. Mice were genotyped by PCR of tail DNA as described previously (10). Experimental animal procedures and protocols were approved by the French Animal Care and Use Committee.

CT images of human patients and mice

Human patients CT images were produced by a 64-slice CT system (LightSpeed VCT; General Electric Medical Systems, Milwaukee, WI, USA). The images were reconstructed in 3D using Carestream PACS v11.0 software (Carestream Health, Rochester, NY, USA). Cephalometric analysis of the mandible was carried on sagittal views of the 3D reconstructions.

Following 15 days of NVP-BGJ398 treatment, *Fgfr3*$^{Y367C/+}$ mice and their control littermates were sacrificed, and the whole heads were imaged using a μCT40 Scanco vivaCT42 (Scanco Medical, Bassersdorf, Switzerland). The following settings were used: integration time: 300 ms, 45 E(kVp), 177 μA. The mandible images were reconstructed in 3D using OsiriX 64-bit version software (Pixmeo, Bernex, Switzerland).

Morphometric analysis

The samples consisted of CT images of patients with ACH and unaffected age-matched individuals, and of high-resolution CT images of 7 P21 *Fgfr3*$^{Y367C/+}$ mice and seven control littermates. Three-dimensional coordinates of 10 landmarks were recorded on the 3D reconstructed mandibles of humans and mice and analyzed with geometric morphometric methods. Standardization for position, scale and orientation was obtained by Procrustes superimposition (62,63), and shape information (Procrustes coordinates) and size (CS (63)) were extracted. Shape information was subsequently analyzed by PCA [for more information on geometric morphometrics applied to craniofacial birth defect, see (31)]. Wireframes are used to visualize the shape differences between positive and negative values of PC 1 corresponding to control and ACH mandibles respectively. Geometric morphometric analyses were run with Morpho J (64).

Whole-mount Alcian blue-alizarin red staining

Mandibles of *Fgfr3*$^{Y367C/+}$ mice and their WT littermates at E16.5, E18.5, P0 and P21 were fixed in 95% ethanol and then stained with Alizarin Red and Alcian Blue, cleared by KOH treatment and stored in glycerol according to standard protocols. Size of the mandibles and the condyles was measured on images captured with an Olympus PD70-IX2-UCB using CellSens software (Olympus). Total length of the mandible as well as the length of the condylar and symphyseal cartilages were measured (identified with the alcian blue staining). The length of the body was calculated as the total length minus the condylar and symphyseal cartilages.

Immunohistochemistry

Mandibles of *Fgfr3*$^{Y367C/+}$ and their WT littermates at E16.5, E18.5, P0 and P21 were fixed in 4% paraformaldehyde at 5 °C for 24 hours and decalcified in 0.5 M EDTA (pH 8.0) overnight or up to 1 week, depending on the age of the mice, and then dehydrated in graded series of ethanol, cleared in xylenes and embedded in paraffin. Five micometre sagittal sections were cut and stained with haematoxylin and eosin (H&E), safranin-O or subjected to immunohistochemical staining using standard protocols using an antibody against Collagen X (1:50 dilution; BIOCYC, Luckenwalde, Germany), FGFR3 (1:250; Sigma-Aldrich Co, St. Louis, MO, USA) or Ki67 (1:3000; Abcam, Cambridge, MA, USA) using the Dako Envision kit (Dako North America, Inc., CA, USA). Images were captured with an Olympus PD70-IX2-UCB microscope (Olympus, Tokyo, Japan), and morphometry was performed with ImageJ software (National Institutes of Health, Bethesda, MD, USA).

Ex vivo experiments

Mandibles from WT and *Fgfr3*$^{Y367C/+}$ E16.5 embryos were dissected and cut at the symphysis to separate the two hemi-mandibles. For each embryo, the two hemi-mandibles were incubated for 5 days in DMEM medium with antibiotics and 0.2% BSA (Sigma), one supplemented with NVP-BGJ398 (100 nM), whereas the other served as control and was supplemented with DMSO (0.1%). The length of the hemi-mandibles was measured at the end of time course, following whole-mount Alcian blue-alizarin red staining.

In vivo experiments

Fgfr3$^{Y367C/+}$ *mice* were 1-day old at treatment initiation and received daily subcutaneous administrations of NVP-BGJ398 at 2 mg/kg body weight or vehicle (HCl 3.15 mM, DMSO 2%) for 15

days. Cartilage and bone analyses were thus performed in 16-day-old male and female mice. Experimental animal procedures and protocols were approved by the French Animal Care and Use Committee.

Statistical analysis

Differences between experimental groups were assessed using analysis of variance or Mann–Whitney test. The significance threshold was set at $P \leq 0.05$. Statistical analyses were performed using GraphPad PRISM (v5) (GraphPad Software Inc., La Jolla, CA, USA). All values are shown as mean ± SD.

Authors' Contributions

M.B.D., D.K.E., Y.H. and L.L.M. designed research. M.B.D, D.K.E., Y.H., V.E., E.G., N.K. and C.B.L. performed research. I.K., M.K. and D.G.P. contributed new reagents. M.Z. and F.D.R. contributed human data. M.B.D., Y.H. and F.D.R. analyzed mouse and human data. M.B.D., D.K.E., Y.H. and L.L.M. prepared the figures and wrote the article.

Conflict of Interest statement. IK, DGP and MK work for Novartis. The other authors have declared that no conflict of interest exists.

Funding

Comité d'interface INSERM/Odontologie (MBD), YH was partly funded by the French National Agency of Research (ANR) through the program "Investissements d'avenir" (ANR-10-LABX-52). This project received a state subsidy managed by the National Research Agency under the "Investments for the Future" program bearing the reference ANR-10-IHU-01, the European Community's Seventh Framework Programme Under grant agreement no. 602300 (Sybil) the Fondation des Gueules Cassées and the Association des Personnes de Petites Tailles. Funding to pay the Open Access publication charges for this article was provided by INSERM U1163.

References

1. Baujat, G., Legeai-Mallet, L., Finidori, G., Cormier-Daire, V. and Le Merrer, M. (2008) Achondroplasia. *Best Pract. Res. Clin. Rheumatol*, **22**, 3–18.
2. Horton, W.A., Hall, J.G. and Hecht, J.T. (2007) Achondroplasia. *Lancet*, **370**, 162–172.
3. Di Rocco, F., Biosse Duplan, M., Heuzé, Y., Kaci, N., Komla-Ebri, D., Munnich, A., Mugniery, E., Benoist-Lasselin, C. and Legeai-Mallet, L. (2014) FGFR3 mutation causes abnormal membranous ossification in achondroplasia. *Hum. Mol. Genet*, **23**, 2914–2925.
4. Rousseau, F., Bonaventure, J., Legeai-Mallet, L., Pelet, A., Rozet, J.M., Maroteaux, P., Le Merrer, M. and Munnich, A. (1994) Mutations in the gene encoding fibroblast growth factor receptor-3 in achondroplasia. *Nature*, **371**, 252–254.
5. Ornitz, D.M. (2005) FGF signaling in the developing endochondral skeleton. *Cytokine Growth Factor Rev.*, **16**, 205–213.
6. Legeai-Mallet, L., Benoist-Lasselin, C., Munnich, A. and Bonaventure, J. (2004) Overexpression of FGFR3, Stat1, Stat5 and p21Cip1 correlates with phenotypic severity and defective chondrocyte differentiation in FGFR3-related chondrodysplasias. *Bone*, **34**, 26–36.
7. Wang, Q., Green, R.P., Zhao, G. and Ornitz, D.M. (2001) Differential regulation of endochondral bone growth and joint development by FGFR1 and FGFR3 tyrosine kinase domains. *Dev. Camb. Engl*, **128**, 3867–3876.
8. Segev, O., Chumakov, I., Nevo, Z., Givol, D., Madar-Shapiro, L., Sheinin, Y., Weinreb, M. and Yayon, A. (2000) Restrained chondrocyte proliferation and maturation with abnormal growth plate vascularization and ossification in human FGFR-3(G380R) transgenic mice. *Hum. Mol. Genet*, **9**, 249–258.
9. Matsushita, T., Wilcox, W.R., Chan, Y.Y., Kawanami, A., Bukulmez, H., Balmes, G., Krejci, P., Mekikian, P.B., Otani, K., Yamaura, I., *et al.* (2008) FGFR3 promotes synchondrosis closure and fusion of ossification centers through the MAPK pathway. *Hum. Mol. Genet*, **18**, 227–240.
10. Pannier, S., Couloigner, V., Messaddeq, N., Elmaleh-Bergès, M., Munnich, A., Romand, R. and Legeai-Mallet, L. (2009) Activating Fgfr3 Y367C mutation causes hearing loss and inner ear defect in a mouse model of chondrodysplasia. *Biochim. Biophys. Acta*, **1792**, 140–147.
11. Komla-Ebri, D., Dambroise, E., Kramer, I., Benoist-Lasselin, C., Kaci, N., Le Gall, C., Martin, L., Busca, P., Barbault, F., Graus-Porta, D., *et al.* (2016) Tyrosine kinase inhibitor NVP-BGJ398 functionally improves FGFR3-related dwarfism in mouse model. *J. Clin. Invest*, 10.1172/JCI83926.
12. Roberts, W.E. and Hartsfield, J.K. (2004) Bone development and function: genetic and environmental mechanisms. *Semin. Orthod*, **10**, 100–122.
13. Dixon, A., Hoyte, D. and Rönning, O. (1997) *Fundamentals of craniofacial growth* Boca Raton: CRC Press.
14. Chen, H., Liu, C.T., Yang, S.S. and Opitz, J.M. (1981) Achondrogenesis: A review with special consideration of achondrogenesis type II (langer-saldino). *Am. J. Med. Genet*, **10**, 379–394.
15. Mansour, S., Offiah, A.C., McDowall, S., Sim, P., Tolmie, J. and Hall, C. (2002) The phenotype of survivors of campomelic dysplasia. *J. Med. Genet*, **39**, 597–602.
16. Schipani, E., Langman, C.B., Parfitt, A.M., Jensen, G.S., Kikuchi, S., Kooh, S.W., Cole, W.G. and Jüppner, H. (1996) Constitutively activated receptors for parathyroid hormone and parathyroid hormone-related peptide in Jansen's metaphyseal chondrodysplasia. *N. Engl. J. Med*, **335**, 708–714.
17. Wilkie, A.O., Slaney, S.F., Oldridge, M., Poole, M.D., Ashworth, G.J., Hockley, A.D., Hayward, R.D., David, D.J., Pulleyn, L.J. and Rutland, P. (1995) Apert syndrome results from localized mutations of FGFR2 and is allelic with Crouzon syndrome. *Nat. Genet*, **9**, 165–172.
18. Lajeunie, E., El Ghouzzi, V., Le Merrer, M., Munnich, A., Bonaventure, J. and Renier, D. (1999) Sex related expressivity of the phenotype in coronal craniosynostosis caused by the recurrent P250R FGFR3 mutation. *J. Med. Genet*, **36**, 9–13.
19. Rice, D.P.C., Rice, R. and Thesleff, I. (2003) Fgfr mRNA isoforms in craniofacial bone development. *Bone*, **33**, 14–27.
20. Yu, K., Karuppaiah, K. and Ornitz, D.M. (2015) Mesenchymal fibroblast growth factor receptor signaling regulates palatal shelf elevation during secondary palate formation: Mesenchymal FGFR Regulates Palatal Shelf Elevation. *Dev. Dyn.*, **244**, 1427–1438.
21. Havens, B.A., Rodgers, B. and Mina, M. (2006) Tissue-specific expression of Fgfr2b and Fgfr2c isoforms, Fgf10 and Fgf9 in the developing chick mandible. *Arch. Oral Biol*, **51**, 134–145.
22. Havens, B.A., Velonis, D., Kronenberg, M.S., Lichtler, A.C., Oliver, B. and Mina, M. (2008) Roles of FGFR3 during morphogenesis of Meckel's cartilage and mandibular bones. *Dev. Biol.*, **316**, 336–349.

23. de Frutos, C.A., Vega, S., Manzanares, M., Flores, J.M., Huertas, H., Martínez-Frías, M.L. and Nieto, M.A. (2007) Snail1 is a transcriptional effector of FGFR3 signaling during chondrogenesis and achondroplasias. *Dev. Cell*, **13**, 872–883.
24. Murray, S.A., Oram, K.F. and Gridley, T. (2007) Multiple functions of Snail family genes during palate development in mice. *Dev. Camb. Engl.*, **134**, 1789–1797.
25. Liu, Z., Lavine, K.J., Hung, I.H. and Ornitz, D.M. (2007) FGF18 is required for early chondrocyte proliferation, hypertrophy and vascular invasion of the growth plate. *Dev. Biol.*, **302**, 80–91.
26. Cohen, M.M., Walker, G.F. and Phillips, C. (1985) A morphometric analysis of the craniofacial configuration in achondroplasia. *J. Craniofac. Genet. Dev. Biol. Suppl.*, **1**, 139–165.
27. Cardoso, R., Ajzen, S., Andriolo, A.R., de Oliveira, J.X. and Andriolo, A. (2012) Analysis of the cephalometric pattern of Brazilian achondroplastic adult subjects. *Dent. Press J. Orthod*, **17**, 118–129.
28. Tuncer, O., Caksen, H., Kirimi, E., Kayan, M., Ataş, B. and Odabaş, D. (2004) A case of thanatophoric dysplasia type I associated with mandibular clefting. *Genet. Couns. Geneva Switz*, **15**, 95–97.
29. Ridgway, E.B., Wu, J.K., Sullivan, S.R., Vasudavan, S., Padwa, B.L., Rogers, G.F. and Mulliken, J.B. (2011) Craniofacial growth in patients with FGFR3Pro250Arg mutation after frontoorbital advancement in infancy. *J. Craniofac. Surg.*, **22**, 455–461.
30. Guagnano, V., Furet, P., Spanka, C., Bordas, V., Le Douget, M., Stamm, C., Brueggen, J., Jensen, M.R., Schnell, C., Schmid, H., *et al.* (2011) Discovery of 3-(2,6-dichloro-3,5-dimethoxy-phenyl)-1-{6-[4-(4-ethyl-piperazin-1-yl)-phenylamino]-pyrimidin-4-yl}-1-methyl-urea (NVP-BGJ398), a potent and selective inhibitor of the fibroblast growth factor receptor family of receptor tyrosine kinase. *J. Med. Chem*, **54**, 7066–7083.
31. Heuzé, Y., Boyadjiev, S.A., Marsh, J.L., Kane, A.A., Cherkez, E., Boggan, J.E. and Richtsmeier, J.T. (2010) New insights into the relationship between suture closure and craniofacial dysmorphology in sagittal nonsyndromic craniosynostosis. *J. Anat*, **217**, 85–96.
32. Lorget, F., Kaci, N., Peng, J., Benoist-Lasselin, C., Mugniery, E., Oppeneer, T., Wendt, D.J., Bell, S.M., Bullens, S., Bunting, S., *et al.* (2012) Evaluation of the therapeutic potential of a CNP analog in a Fgfr3 mouse model recapitulating achondroplasia. *Am. J. Hum. Genet*, **91**, 1108–1114.
33. Frommer, J. and Margolies, M.R. (1971) Contribution of Meckel's cartilage to ossification of the mandible in mice. *J. Dent. Res.*, **50**, 1260–1267.
34. Shimo, T., Kanyama, M., Wu, C., Sugito, H., Billings, P.C., Abrams, W.R., Rosenbloom, J., Iwamoto, M., Pacifici, M. and Koyama, E. (2004) Expression and roles of connective tissue growth factor in Meckel's cartilage development. *Dev. Dyn. Off. Publ. Am. Assoc. Anat.*, **231**, 136–147.
35. Jonquoy, A., Mugniery, E., Benoist-Lasselin, C., Kaci, N., Le Corre, L., Barbault, F., Girard, A.L., Le Merrer, Y., Busca, P., Schibler, L., *et al.* (2012) A novel tyrosine kinase inhibitor restores chondrocyte differentiation and promotes bone growth in a gain-of-function Fgfr3 mouse model. *Hum. Mol. Genet*, **21**, 841–851.
36. Kronenberg, H.M. (2003) Developmental regulation of the growth plate. *Nature*, **423**, 332–336.
37. Delezoide, A.L., Benoist-Lasselin, C., Legeai-Mallet, L., Le Merrer, M., Munnich, A., Vekemans, M. and Bonaventure, J. (1998) Spatio-temporal expression of FGFR 1, 2 and 3 genes during human embryo-fetal ossification. *Mech. Dev*, **77**, 19–30.
38. Ishizeki, K., Saito, H., Shinagawa, T., Fujiwara, N. and Nawa, T. (1999) Histochemical and immunohistochemical analysis of the mechanism of calcification of Meckel's cartilage during mandible development in rodents. *J. Anat.*, **194**, 265–277.
39. Sakakura, Y. (2010) Role of Matrix Metalloproteinases in Extracellular Matrix Disintegration of Meckel's Cartilage in Mice. *J. Oral Biosci*, **52**, 143–149.
40. Pannier, S., Mugniery, E., Jonquoy, A., Benoist-Lasselin, C., Odent, T., Jais, J.P., Munnich, A. and Legeai-Mallet, L. (2010) Delayed bone age due to a dual effect of FGFR3 mutation in Achondroplasia. *Bone*, **47**, 905–915.
41. Pirttiniemi, P., Peltomäki, T., Müller, L. and Luder, H.U. (2009) Abnormal mandibular growth and the condylar cartilage. *Eur. J. Orthod.*, **31**, 1–11.
42. Shen, G. and Darendeliler, M.A. (2005) The adaptive remodeling of condylar cartilage—. *A Transition from Chondrogenesis to Osteogenesis. J. Dent. Res.*, **84**, 691–699.
43. Obwegeser, H.L. (2001) *Mandibular Growth Anomalies Springer Berlin Heidelberg*. Berlin, Heidelberg.
44. Vajo, Z., Francomano, C.A. and Wilkin, D.J. (2000) The molecular and genetic basis of fibroblast growth factor receptor 3 disorders: the achondroplasia family of skeletal dysplasias, Muenke craniosynostosis, and Crouzon syndrome with acanthosis nigricans. *Endocr. Rev*, **21**, 23–39.
45. Naski, M.C., Colvin, J.S., Coffin, J.D. and Ornitz, D.M. (1998) Repression of hedgehog signaling and BMP4 expression in growth plate cartilage by fibroblast growth factor receptor 3. *Dev. Camb. Engl*, **125**, 4977–4988.
46. Yasuda, T., Nah, H.D., Laurita, J., Kinumatsu, T., Shibukawa, Y., Shibutani, T., Minugh-Purvis, N., Pacifici, M. and Koyama, E. (2012) Muenke syndrome mutation, FgfR3P^{244}R, causes TMJ defects. *J. Dent. Res.*, **91**, 683–689.
47. Harada, Y. and Ishizeki, K. (1998) Evidence for transformation of chondrocytes and site-specific resorption during the degradation of Meckel's cartilage. *Anat. Embryol. (Berl.)*, **197**, 439–450.
48. Bi, W., Huang, W., Whitworth, D.J., Deng, J.M., Zhang, Z., Behringer, R.R. and de Crombrugghe, B. (2001) Haploinsufficiency of Sox9 results in defective cartilage primordia and premature skeletal mineralization. *Proc. Natl. Acad. Sci. U. S. A*, **98**, 6698–6703.
49. Wang, Y., Spatz, M.K., Kannan, K., Hayk, H., Avivi, A., Gorivodsky, M., Pines, M., Yayon, A., Lonai, P. and Givol, D. (1999) A mouse model for achondroplasia produced by targeting fibroblast growth factor receptor 3. *Proc. Natl. Acad. Sci. U. S. A*, **96**, 4455–4460.
50. Cooper, K.L., Oh, S., Sung, Y., Dasari, R.R., Kirschner, M.W. and Tabin, C.J. (2013) Multiple phases of chondrocyte enlargement underlie differences in skeletal proportions. *Nature*, **495**, 375–378.
51. Wang, Y., Nishida, S., Sakata, T., Elalieh, H.Z., Chang, W., Halloran, B.P., Doty, S.B. and Bikle, D.D. (2006) Insulin-like growth factor-I is essential for embryonic bone development. *Endocrinology*, **147**, 4753–4761.
52. Sugito, H., Shibukawa, Y., Kinumatsu, T., Yasuda, T., Nagayama, M., Yamada, S., Minugh-Purvis, N., Pacifici, M. and Koyama, E. (2011) Ihh signaling regulates mandibular symphysis development and growth. *J. Dent. Res.*, **90**, 625–631.
53. Iwata, T., Chen, L., Li, C., Ovchinnikov, D.A., Behringer, R.R., Francomano, C.A. and Deng, C.X. (2000) A neonatal lethal mutation in FGFR3 uncouples proliferation and

differentiation of growth plate chondrocytes in embryos. *Hum. Mol. Genet.*, **9**, 1603–1613.
54. Narayana, J. and Horton, W.A. (2015) FGFR3 biology and skeletal disease. *Connect. Tissue Res.*, **56**, 427–433.
55. Legeai-Mallet, L., Benoist-Lasselin, C., Delezoide, A.L., Munnich, A. and Bonaventure, J. (1998) Fibroblast growth factor receptor 3 mutations promote apoptosis but do not alter chondrocyte proliferation in thanatophoric dysplasia. *J. Biol. Chem*, **273**, 13007–13014.
56. Mugniery, E., Dacquin, R., Marty, C., Benoist-Lasselin, C., de Vernejoul, M.C., Jurdic, P., Munnich, A., Geoffroy, V. and Legeai-Mallet, L. (2012) An activating Fgfr3 mutation affects trabecular bone formation via a paracrine mechanism during growth. *Hum. Mol. Genet*, **21**, 2503–2513.
57. Benko, S., Fantes, J.A., Amiel, J., Kleinjan, D.J., Thomas, S., Ramsay, J., Jamshidi, N., Essafi, A., Heaney, S., Gordon, C.T., *et al.* (2009) Highly conserved non-coding elements on either side of SOX9 associated with Pierre Robin sequence. *Nat. Genet*, **41**, 359–364.
58. Berraquero, R., Palacios, J. and Rodríguez, J.I. (1992) The role of the condylar cartilage in mandibular growth. A study in thanatophoric dysplasia. *Am. J. Orthod. Dentofac. Orthop.*, **102**, 220–226.
59. Cottrell, D.A., Edwards, S.P. and Gotcher, J.E. (2012) Surgical correction of maxillofacial skeletal deformities. *J. Oral Maxillofac. Surg.*, **70**, e107–e136.
60. Shirley, E.D. and Ain, M.C. (2009) Achondroplasia: manifestations and treatment. *J. Am. Acad. Orthop. Surg.*, **17**, 231–241.
61. Metzger, D., Clifford, J., Chiba, H. and Chambon, P. (1995) Conditional site-specific recombination in mammalian cells using a ligand-dependent chimeric Cre recombinase. *Proc. Natl Acad. Sci. USA*, **92**, 6991–6995.
62. Rohlf, F.J. and Slice, D. (1990) Extensions of the procrustes method for the optimal superimposition of landmarks. *Syst. Biol.*, **39**, 40–59.
63. Dryden, I. and Mardia, K. (1998) *Statistical Shape Analysis*. Wiley, Chichester.
64. Klingenberg, C.P. (2011) MorphoJ: an integrated software package for geometric morphometrics. *Mol. Ecol. Resour.*, **11**, 353–357.